Journal of Enzyme Inhibition and Medicinal Chemistry, 2002 Vol. 17 (4), pp. 235–246

Characterization of Competitive Inhibitors for the Transferase Activity of *Pseudomonas aeruginosa* Exotoxin A*

SOUZAN ARMSTRONG[a], JIA-HE LI[b], JIE ZHANG[b] and A. ROD MERRILL[a,†]

[a]*Guelph-Waterloo Centre for Graduate Work in Chemistry and Biochemistry, Department of Chemistry and Biochemistry, University of Guelph, Guelph, Ont., Canada N1G 2W1;* [b]*Guilford Pharmaceuticals, Baltimore, MD 21224, USA*

(Received 27 March 2002)

A series of small, nonpolar compounds were tested for their ability to inhibit the ADP-ribosyl transferase activity of *Pseudomonas aeruginosa* exotoxin A. The IC_{50} values for the compounds tested ranged from 87 nM to 484 μM for NAP and CMP12, respectively. It was demonstrated that NAP was a competitive inhibitor of the ADPRT reaction for the NAD^+ substrate with a K_i of 45 ± 5 nM, which was in good agreement with the dissociation constant determined independently (K_D = 56 ± 6 nM). The IC_{50} value for NAP was 87 ± 12 nM, which strongly correlated with the K_i and K_D values. Furthermore, NAP was shown to noncovalently associate with the exotoxin A active site using exhaustive dialysis, NMR, and electrospray mass spectrometry. Finally, a computer molecular model using the X-ray structure of the substrate-bound toxin was generated with NAP bound to the active site of exotoxin A at the nicotinamide-binding site. This model is consistent with the X-ray structure of the catalytic domain of poly-ADP-ribose polymerase complexed with 4-amino-naphthalimide (Compound 4) that was included in this study.

Keywords: ADP-ribosyl transferase; *Pseudomonas aeruginosa* exotoxin A; Computer molecular model; ADPRT; PARPS

INTRODUCTION

Pseudomonas aeruginosa (PA) is a motile, aerobic, Gram-negative rod bacterium that is commonly found in soil and ground water. It is capable of growing in low nutrient environments and has the ability to use a variety of organic compounds as carbon sources and electron donors.[1] This organism is an opportunistic human pathogen that is among the six most frequently encountered pathogens in nosocomial infections, the third most common bacterial isolate from blood borne infections, and is the most frequent cause of nosocomial pneumonia.[2] It can also cause urinary tract infections, ear, nose, and throat infections, and cardiovascular and blood-stream infections. Generally, however, PA is known to cause diseases in patients with compromised host defenses, such as burn victims, and those suffering from AIDS, cancer, or cystic fibrosis. PA synthesizes a number of extracellular toxic products believed to be involved in the pathogenesis of these infections; however, the most potent virulence factor produced by PA is a 66 kDa protein, exotoxin A (ETA). Although ETA expression is not normally required for PA growth and viability, it is an important contributor to the virulence of PA, as demonstrated during pulmonary infection in an immunologically naïve but competent neonatal mouse model.[3]

Pseudomonas aeruginosa exotoxin A (ETA) is a secreted bacterial toxin that gains entry into the host eukaryotic cell by receptor-mediated endocytosis.[4]

*Supported by the Canadian Cystic Fibrosis Research Foundation (CCFF) and the Canadian Institutes of Health Research (CIHR).

†Corresponding author. Tel.: +1-519-824-4120 ext.: 3806. Fax: +1-519-766-1499. E-mail: merrill@chembio.uoguelph.ca

Abbreviations: ADPRT, ADP-ribosyltransferase; β-TAD^+, beta-methylene-thiazole-4-carboxamide adenine dinucleotide; DMSO, dimethyl sulfoxide; DT, diphtheria toxin; eEF-2, eukaryotic elongation factor-2; ES-MS, electrospray mass spectrometry; ETA, *P. aeruginosa* exotoxin A; IC_{50}, inhibitory concentration for 50% inhibition of enzyme activity; k_{cat}, catalytic rate constant; K_D, dissociation constant; K_M, Michaelis constant; NAP, 1,8-naphthalimide; NATA, *N*-acetyltryptophanamide; PA, *Pseudomonas aeruginosa*; PARP1, poly-(ADP-ribose) polymerase-1; PARP1-CF, poly-(ADP-ribose) polymerase C-terminal fragment; PARPs, poly-(ADP-ribose) polymerases; PE24, *P. aeruginosa* exotoxin A C-terminal catalytic fragment; SDS-PAGE, sodium dodecyl sulfate polyacrylamide gel electrophoresis; TRIS, Tris(hydroxy-methyl) aminomethane

ISSN 1475-6366 print/ISSN 1475-6374 online © 2002 Taylor & Francis Ltd
DOI: 10.1080/1475636021000010914

It utilizes the α_2-macroglobulin receptor complex found on the external side of the plasma membrane of many eukaryotic cells.[5] The toxin gains entry into the cytoplasm of the host by route of the retrograde pathway[6,7] and effectively slows protein synthesis by transferring the ADP-ribosyl moiety of NAD^+ onto the diphthamide residue of endogenous eukaryotic elongation factor-2 (eEF-2),[8] a highly conserved and essential catalytic protein factor that functions at the ribosome.[9] The C-terminal one-third of the toxin contains the catalytic domain (PE24) that possesses the ribosyltransferase activity.[10] The X-ray structure of PE24 was determined with the hydrolysis products of NAD^+ bound within the active site[11] and later with an NAD^+ analogue, β-methylene-thiazole-4-carboxamide adenine dinucleotide (β-TAD^+).[12] The PE24 enzyme shows common functional and structural properties with members of the mono-ADPRT family, including diphtheria toxin, cholera toxin, pertussis toxin, *E. coli* heat labile endotoxin, and others.[13] Furthermore, the group of poly (ADP-ribose) polymerase enzymes (PARPs), located in the nucleus of most eukaryotes, shows significant structural homology with the catalytic domains of the bacterial toxins.[14] This whole family represents an unique class (Class 7) of NAD^+-binding enzymes that bind NAD^+ in a compact configuration that places strain on the N-glycosidic bond.[15]

This paper reports the kinetic characterization of a group of inhibitor compounds designed as potential NAD^+competitive inhibitors. These compounds serve as competitive inhibitors for the NAD^+ substrate of ETA and, in this paper, we provide experimental and molecular modeling evidence for the structure of the transition state for the ADPRT reaction catalyzed by ETA. Unfortunately, evidence for the structure of the transition state of this reaction has been impeded by the difficulty in obtaining structural data on the protein substrate, eEF-2, for both ETA and DT. However, results shown herein implicate the naphthalimide series of compounds as a good template on which to build potent transition-state analogues, which may provide essential information concerning the catalytic mechanism for this enzyme class. In addition, insights into the transition-state species for these enzymes may provide the basis for the design and development of useful inhibitors and therapeutic compounds for the treatment of bacterial diseases as well as heart attack and stroke patients.[16,17]

MATERIALS AND METHODS

Molecular Modeling

The molecular modeling package Sybyl (version 6.7, Tripos Associates Inc.) was used on a Silicon Graphics Indigo2 R4400 XZ workstation to generate the molecular model shown in Figure 4. The full coordinates of the catalytic domain of PE24/β-TAD complex[12] (PDB entry, 1AER) were obtained from the Brookhaven Protein Data Bank (PDB; http://www.rcsb.org/pdb/). The structure of 1,8-naphthalimide (NAP) was built using the Sketch function within Sybyl and was then geometry optimized using the Tripos force field. The structure of NAP was then superimposed onto β-TAD in two different orientations (two models) using the Fit Atom command and selecting the atoms of the thiazole ring as the point of reference for the least squares fit. Following the docking procedure, the geometry of the models was optimized using the Anneal function. The standard Sybyl energy minimizer, MAXIMIN2, was used under the following (default) conditions. If the force for any atom exceeded 1000 kcal/mol, then an atom-by-atom Simplex minimization was performed until all forces fell below this threshold. After this threshold was established, minimization then proceeded until the convergence criterion on a root-mean squared force over all atoms of less than 0.05 kcal/mol was reached. Non-bonded interactions between substructures (residues) more than 8.0 Å apart were neglected. The electrostatic interactions were included based on empirically assigned partial atomic charges[18] in all of the minimizations. The use of the Anneal function allows the MAXMIN2 energy minimization of a subset region around the site where the inhibitor is bound to the protein. There are three distinct regions of the protein defined during an anneal minimization. The "hot" region is defined as a molecular zone including all residues around the bound inhibitor. The inhibitor and the amino acid residues in the "hot" region are energy minimized through conformational and geometrical changes. The "interesting" region contains all of the amino acid residues within 12 Å of the "hot" region. This region is not subject to energy minimization during the anneal process, but the effect of the atoms of the "interesting" region on the atoms in the "hot" region is considered during annealing. The third region is defined as all of the amino acid residues outside of the "hot" and "interesting" regions. This region is held static during the minimization and is ignored during computations.

Sequence Alignment

The primary sequences for a subset sequence of the C-terminal catalytic domains of ETA, DT and PARP1 were aligned using CLUSTAL W (1.81) found at *http://www2.ebi.ac.uk/clustalw/* in the multiple sequence alignment mode.

ADPRT Assay

A typical assay as previously characterized[10] (70 μL total volume) contained ϵ-NAD^+ (desired concentration), eEF-2 (20 μM) and buffer (20 mM Tris.HCl, pH 7.8) in a 3 mm pathlength ultramicrocuvette (Helma Inc., Concord, ON) placed in the sample chamber of a PTI Alphascan-2 fluorometer (Photon Technology International Inc., South Brunswick, NJ). Following temperature equilibration for 10 min, the reaction was initiated by the introduction of PE24 (5 nM). The reaction was monitored by recording the increase in fluorescence intensity with time (excitation 305 nm, emission through a 309 nm cut-off filter). These experiments were performed over a wide range (0–700 μM) of ϵ-NAD^+, using appropriate aliquots of a 57 mM stock solution of this compound in the above buffer. In all experiments, the KCl concentration was kept at 50 mM concentration.

ϵ-AMP Standard Curve and Assay Calibration

A stock solution of 44.7 mM ϵ-AMP in distilled water was prepared ($\varepsilon_M^{265} = 10,000\,M^{-1}\,cm^{-1}$) along with a series of standards, containing 0–7 μM ϵ-AMP in buffer (20 mM Tris, pH 7.8). The fluorescence emission of each standard was measured and a standard curve constructed, which was used to calibrate the enzyme-catalyzed reaction rate.

Kinetic Analysis

Determination of K_M and V_{max} for PE24 involved measurement of initial rates at ten different concentrations of substrates (50–700 μM ϵ-NAD^+). When the concentration of ϵ-NAD^+ was varied, the eEF-2 concentration was kept constant at 20 μM. The activity at each substrate concentration was determined in triplicate and all the experiments were performed at least three times.

Dose-response Determination of Naphthalimide Compounds

The compounds tested in this study were either commercially available from Sigma or were provided by Guilford Pharmaceuticals (Baltimore, MD, for more details see review paper [19]) (see Figure 1). The ADPRT activity of PE24 in the presence of each of the inhibitors was measured in a similar fashion as that discussed in the *ADPRT assay* above. In these studies, the ϵ-NAD^+ and eEF-2 concentrations in the assay medium were held at 500 μM and 20 μM (V_{max}), respectively. The reactions were initiated by the addition of PE24 (5 nM), which had been pre-incubated (10 min) with the desired concentration of inhibitor (0–100 μM). The data on inhibitor concentration dependence of ADPRT activity were analyzed by nonlinear regression curve fitting using Origin 6.1 (OriginLab, Northhampton, MA). The data were fit to the equation below,

$$Y = A_1(A_2 - A_1/1 + 10^{([I]-\log[IC_{50}])})$$

where Y is the observed activity measured in the presence of various concentrations of inhibitors, and [I] is the concentration of inhibitor. A_1 is the loss of activity in the presence of high concentration of inhibitor, and A_2 is the activity in the absence of inhibitor. IC_{50} is the concentration of inhibitor that reduces the activity of the enzyme by 50%. The maximum concentration of dimethyl sulfoxide (DMSO) in the reaction assays was 0.2%, and control experiments verified that the enzyme ADPRT activity was not affected by this concentration of DMSO. All experiments were carried out at least two times, with samples measured in triplicate.

Determination of Binding Affinity of Naphthalimide Compounds to PE24

The quenching of the intrinsic protein fluorescence of the tryptophan residues within PE24 was used to determine the binding constant (K_D) for each of the inhibitors. The fluorescence quenching of PE24 was measured as a function of the concentration of inhibitor(s). Triplicate reactions were performed over a concentration range of 0–5 μM for all the compounds, except CMP11 (0–500 μm), in the presence of PE24 at 25°C in an initial volume of 600 μL. PE24 was in 20 mM Tris, pH 7.9 containing 50 mM NaCl for all the assays. Samples were excited at 295 nm (4 nm slit width), and the fluorescence intensity was measured over a range of 305–450 nm (4 nm slit width) in the PTI fluorometer. The final concentration of toxin used in the experiments ranged from 5–20 nM. All the measurements were corrected for buffer contributions to the signal.

Dialysis Experiments

A solution of NAP in DMSO-ethanol mixture (9.0 mM) was mixed with a solution of PE24 in 20 mM TRIS–HCl, pH 7.9 containing 50 mM NaCl (17.5 μM) such that the molar ratio of PE24: NAP was maintained at 1:100. At this ratio the ADPRT activity of PE24 was significantly reduced. A mixture of PE24 with DMSO-ethanol solution served as the control for this experiment. An aliquot of each sample was taken for the measurement of ADPRT activity prior to dialysis. Each of the samples was exhaustively dialyzed in 4L of the above-mentioned buffer at 4°C over 4 days. After dialysis, the concentration of samples was determined in order to compensate for the dilution effects during dialysis, and the ADPRT activity of the samples was measured.

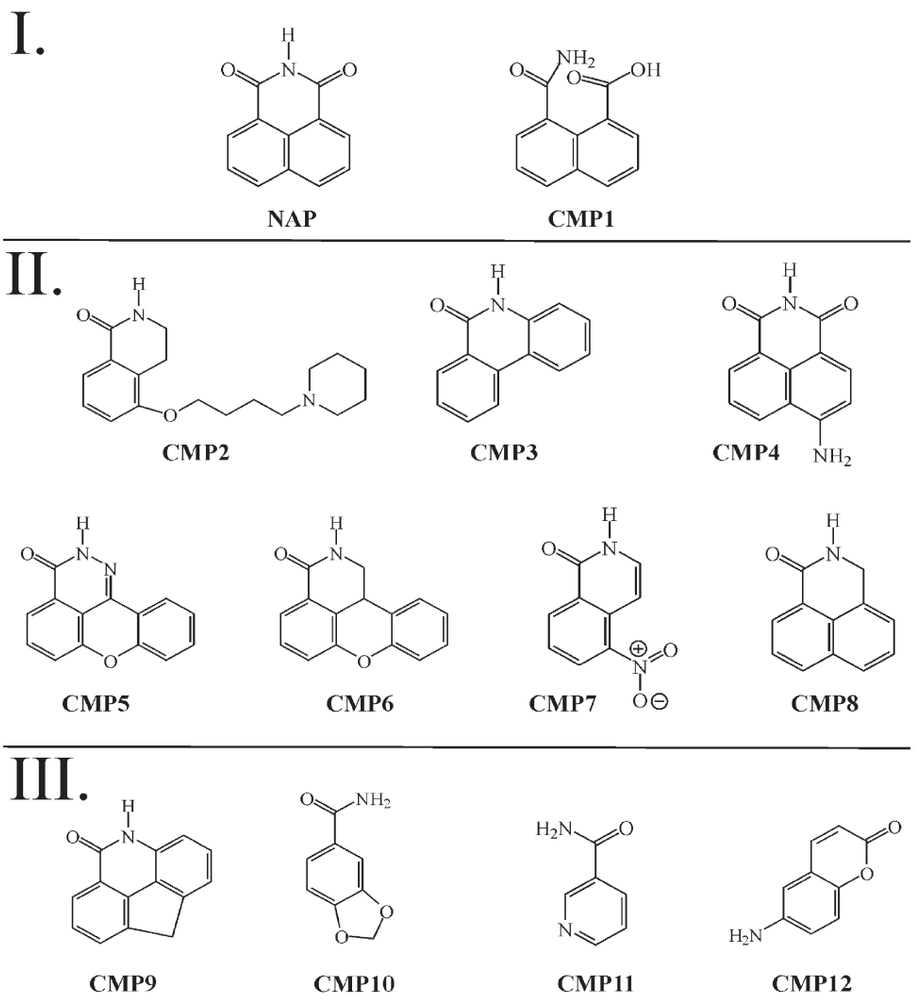

FIGURE 1 *Chemical structures of the ADPRT inhibitors.* The inhibitors against ADPRT activity of exotoxin A are grouped into three categories according to their IC_{50} values. Group I includes compounds that possess nanomolar IC_{50} values, Group II compounds have IC_{50} values that range from 1 μM to 12 μM and Group III compounds exhibited IC_{50} values between 20 and 484 μM.

ES-MS Analysis

A solution of NAP in DMSO-ethanol mixture (4.4 mM) was mixed with a solution of PE24 in 20 mM TRIS–HCl, pH 7.9 containing 50 mM NaCl such that the molar ratio of PE24: NAP was maintained at 1:100. The mixture was lyophilized prior to analysis by electrospray mass spectrometry (ES-MS) conducted at the Chemistry Department at the University of Waterloo. The protein samples were run on a Micromass Quatro II mass spectrometer (Micromass, Manchester, England) fitted with an electrospray source. Flow injection analysis was used with the carrier solvent consisting of 50:50 acetonitrile and water with 0.1% trifluoracetic acid. Approximately 10% methanol was added to the protein samples, which were in distilled water and 5–10 μL of the sample solution was injected. Each sample required from 8–20 scans and the data was processed using MassLynx™ Ver 2.0 and the Maximum Entropy Software package supplied with the instrument.

Kinetic Analysis of Inhibition of ADPRT Activity by NAP

A NAP stock solution was prepared in DMSO and appropriate dilutions of the stock were prepared using ethanol as a co-solvent with buffer (0.2% final). The ADPRT assay was performed at 25°C in 20 mM TRIS–HCl, pH 7.9 containing 50 mM NaCl, as described above. In these studies, the eEF-2 concentration in the assay medium was held at 20 μM, while the concentration of ε-NAD^+ was varied in the range 0–500 μM. The reactions were initiated by the addition of PE24 (20 nM), which had been pre-incubated (10 min) with the desired concentration of

inhibitor (0–1 μM). The data was analyzed by linear regression analysis of Lineweaver-Burk (LB) plots and K_i value was determined using both Dixon plots, as well as secondary plots of the slope of the LB plots versus inhibitor concentrations.

RESULTS

Inhibitor Structures

The parent compound, NAP, has previously been shown to have inhibitory activity against both mono-ADPRTs and PARPs,[20,21] but the inhibition kinetics and the mechanism of action of NAP and related compounds against the former enzyme class has not been well characterized. A small group of inhibitors related to NAP were utilized in this study as a result of the availability of a library of previously synthesized compounds from Guilford Pharmaceuticals (Baltimore, MD;[19]). The structures of the compounds used in this study are shown in Figure 1. Common features of this group of heterocyclic compounds include an aromatic planar core with amide, imide, carbonyl, carboxyl or nitro substituents. It is evident from their chemical structures that this family consists of NAD-like compounds that may be considered as likely candidates for competitive inhibitors with NAD^+ for the enzyme's active site. More specifically, these inhibitors mimic nicotinamide and likely bind into the nicotinamide-binding pocket of the enzyme (A.R. Merrill, unpublished observations). CMP1 is a compound that results from partial hydrolysis of NAP and is a substituted naphthalene (8-amido, 1-carboxynaphthalene). CMP2 is a substituted isoquinoline (5-(4-[N-piperidinyl]butoxy)1-isoquinoline) and CMP3 is a piperidone with two phenyl rings fused at the C-5 and C-6 positions. The CMP4 structure is 4-amino NAP and has been quite well characterized against the PARP family, including the determination of a crystal structure with the inhibitor bound within the chicken PARP-CF enzyme.[22] CMP5 is a substituted xanthene (8,9-azinone xanthene). CMP6 is a xanthene substituted at the C-8 and C-9 positions with carbon-linked amide bridge and CMP7 is 5-nitro-1-isoquinolinone. CMP8 is a derivative of NAP that lacks a carbonyl at the C-6 position of the nitrogen ring. CMP9 is fluorene with a 1,8-amide bridge and CMP10 is benzamide with a 3,4-methylene dioxy bridge. CMP11 is 3-amido-pyridine or nicotinamide, one of the products of the ADPRT reaction and CMP12 is a substituted coumarin (6-amino coumarin-2-one).

Sequence Comparison of ETA with PARP1 and DT

Selected regions of the primary sequence of the catalytic domain of ETA, PE24, were aligned with those of DT and PARP1 in order to deduce any correlations between conserved sequence elements and inhibitor-binding subsites and the results are shown in Figure 2. There are a number of common clusters within the three protein sequences (all H-class members of the ADPRT family[14]), which show significant homology that is correlated with catalytic function. Near the N-terminus of PE24 a tri-residue sequence, Y/W-H-G, is located that includes a catalytically important His residue (His 440) that is believed to be involved in the transfer of the ADP-ribose moiety to the eEF-2 protein substrate.[23,24] The His 440 residue is conserved among the H-class of ADPRT enzymes, but is replaced with an Arg at this position in R-class members of this family.[14] The next significant sequence cluster includes Tyr 470 in ETA that is again conserved within H-class members of the ADPRT family, but is an aromatic (shifted by 1 residue towards the N-terminus) in the R-class members. Among the three H-class members shown in Figure 2, the motif for this cluster is R/K-G-H_B-Y-X-H_L-H_L (with H_B and H_L referring to a hydrophobic and hydrophilic residue, respectively) and this region is a binding subsite for the nicotinamide portion of NAD^+ with important aromatic–aromatic ring stacking between Tyr 470 and the pyridine ring of NAD^+.[25,12] The third sequence cluster includes Tyr 481—not conserved within the R-class—and the motif is G/N-Y-X-X-D/T-H_L-E/Q, which also forms part of the wall of the nicotinamide-binding pocket, but plays a role in transition-state stabilization for both DT and ETA.[26] The fourth major group involves a small sequence cluster beginning at Ala 519, H_L-A/L-P/T-E/D-P/A, that appears to play an important folding role in the catalytic domain (A.R. Merrill, unpublished observations). The last cluster is a β-strand in which is located E-553, an essential conserved catalytic residue found in all members of the ADPRT family.[14]

Quenching of Intrinsic Trp Fluorescence of PE24 by ADPRT Inhibitors

All of the inhibitors shown in Figure 1 caused a decrease in the PE24 Trp fluorescence upon binding with the enzyme. Figure 3a shows a typical fluorescence quench curve for the intrinsic Trp fluorescence of PE24 upon the addition of NAP at increasing concentrations. These data indicate that all members of this group of inhibitors including NAP bind within the active site of the PE24 enzyme and in this respect behaves very similar to the NAD^+ substrate.[27] The data in Figure 3b indicate that the binding of NAP is specific and saturable, which was also found to be the case for all of the inhibitors shown in Figure 1 although considerable variability was observed for the strength of the binding

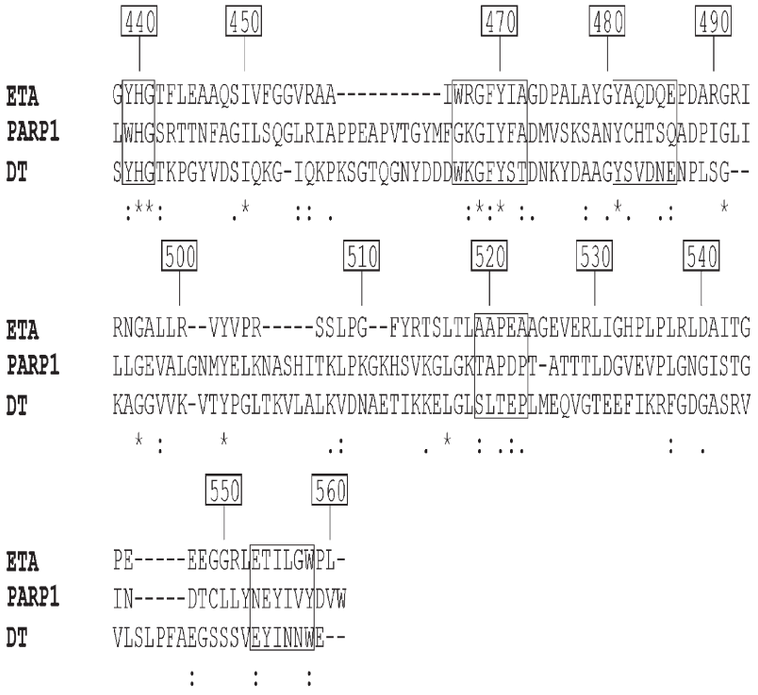

FIGURE 2 *Sequence alignment of selected portions of the C-terminal catalytic domains of Pseudomonas aeruginosa exotoxin A, chicken PARP1, and Cornebacterium diphtheriae diphtheria toxin*. The sequences were taken from the NCBI site with accession numbers CAC38944, P00588, and P26446, respectively. The sequence numbering is according to the full length exotoxin A sequence. [22] Sequence alignment was conducted as described in *Materials and Methods* with conserved residues (*), partially homologous (·), and fully homologous residues (:) indicated. Homologous segments within the three sequences are bounded with a rectangle.

interaction with PE24 and the number of binding sites (Table I).

Molecular Model of Bound NAP

Figure 4 shows the molecular model of NAP bound within the active site of PE24. The inhibitor was positioned within the active site using the known structure of β-TAD$^+$ bound within the PE24 active site[12] and the thiazole ring of the NAD$^+$ analogue as the reference point (corresponding to the pyridine ring of NAD$^+$ as observed within the DT-NAD$^+$ x-ray structure;[15] see *Materials and Methods* for further details). Furthermore, attention was paid to the previously determined X-ray structure of the catalytic domain of chicken PARP complexed with 4-amino-NAP, CMP4[22] (Figure 1). The NAP molecule shown in Figure 4 is nestled between Tyrs 470 and 481 and is positioned with its naphthalene moiety centered where the thiazole ring of β-TAD$^+$ is found in the β-TAD$^+$—PE24 complex.[12] Another model was attempted with NAP oriented 180 degrees to that shown in Figure 4 but it was eliminated based on the preferential alignment of the N atoms within the thiazole and piperidine rings of β-TAD$^+$ and NAP, respectively, for the structure shown in Figure 4. An analysis of a 4 Å sphere surrounding the N atom within NAP indicated that the adjacent residues within PE24 include: His 440, Gly 441, Tyr 470, Ile 471, Ala 472, Leu 477, Ala 478, Tyr 481 and Glu 553. As expected, these residues provide the walls of the nicotinamide-binding pocket for the NAD$^+$ substrate during catalysis, which is in general agreement with the inhibitor complexes of the PARP1 catalytic domain.[22] In this orientation, prospective H-bonds within the NAP—PE24 complex include His 440 side chain and/or the N-H backbone of Gly 441 with the carbonyl at C1 of NAP.

Inhibition of ADPRT and IC_{50} Values

The extent of inhibition by the small family of related inhibitor compounds (Figure 1) is shown in Table I. The IC_{50} values for these compounds ranged from 87 nM (NAP) to more than 100 μM (CMP10). The compounds shown in Figure 1 can be grouped into three categories according to their potency against the ADPRT activity of PE24. Group 1 includes NAP (IC_{50}, 87 ± 12 nM) and CMP1 (IC_{50}, 195 ± 30 nM). Group 2 compounds ranged in potency from 1.0 μM to 12 μM for IC_{50} values and include CMP2 (1.0 ± 0.3 μM), CMP3 (1.0 ± 0.4 μM), CMP4 (1.5 ± 0.2 μM), CMP5 (>5 μM), CMP6 (7.0 ± 2.0 μM), and CMP7 (12 ± 3 μM). The third group includes compounds with IC_{50} values that range from 20 to 484 μM and its members are CMP8

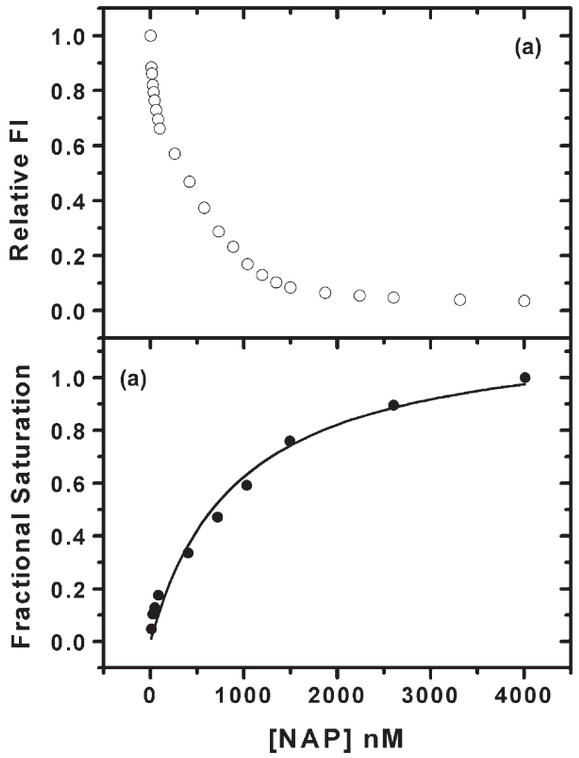

FIGURE 3 *Binding of NAP to PE24 by quenching of intrinsic protein fluorescence. (a) Quench curve for the titration of PE24 with NAP. (b) Binding isotherm for NAP association with PE24.* The titration was conducted in 20 mM Tris–HCl, 50 mM NaCl, pH 7.9 at 25°C using 1.25 μM PE24. The fluorescence excitation was at 295 nm with fluorescence emission at 340 nm (4 nm bandpasses for both excitation and emission). The data were corrected for the dilution effect.

(>20 μM), CMP9 (121 ± 15 μM), CMP10 (>100 μM), CMP11 (139 ± 15 μM), and CMP12 (484 ± 35 μM).

Inhibitor Binding (K_D) to PE24

The change in the intrinsic Trp fluorescence of PE24 was used to characterize the binding of the inhibitor to the toxin-enzyme (Table I). Upon the occupancy of the active site, the various inhibitor compounds significantly quenched the intrinsic Trp fluorescence of the protein (data not shown) in a manner similar with previous binding data for NAD^+ and toxin.[27,29] The dissociation constants for the various inhibitor compounds are shown in Table I. In some cases the binding data curves could not be fit to the equation for a single site model but, instead, were fit to a two-site binding equation (see *Materials and Methods*). K_{D1} values for the inhibitors ranged from very weak and barely detectable binding (CMP5) to specific, tight binding (CMP8, $K_{D1} = 3.0 \pm 0.5$ nM). For most of the inhibitors there was a reasonable correlation between the K_{D1} value and the extent of inhibition. However, there was one major exception. CMP8 exhibited strong binding to the toxin (K_{D1},

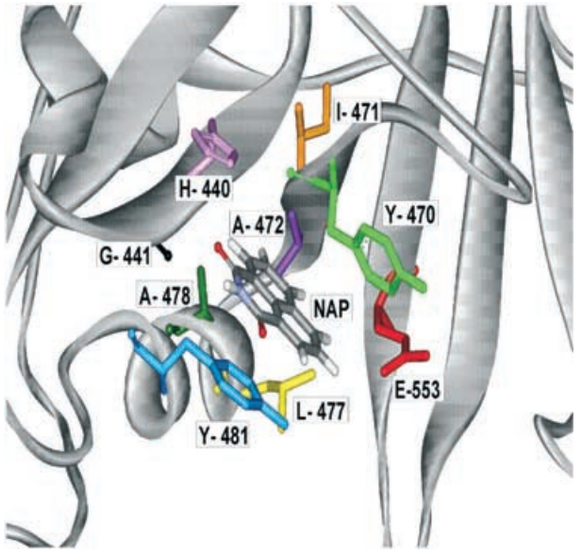

FIGURE 4 *Model for NAP bound within the active site of PE24.* The model was prepared with the molecular modeling package Sybyl (version 6.7, Tripos Associates Inc.) on a Silicon Graphics Indigo2 R4400 XZ workstation. Some of the amino acid residues that line the wall of the nicotinamide-binding pocket are shown as stick drawings. H-440 is shown in pink, G-441 in black, Y-470 in light green, I-471 in orange, A-472 in purple, L-477 in yellow, A-478 in dark green, Y-481 in blue, and E-553 in shown in red. The inhibitor, 1,8-naphthalmide, is also rendered as a stick drawing with the conventional color scheme for the atoms and the protein backbone is shown in grey. The full coordinates of the catalytic domain of PE24/β-TAD complex [12] PDB entry, 1AER) was obtained from the Brookhaven Protein Data Bank (PDB, http:www.rcsb.org/pdb).

3.0 ± 0.5 nM) yet was largely ineffective as an ADPRT inhibitor ($IC_{50} > 20$ μM), suggesting that this inhibitor did not prevent binding of the NAD^+ substrate. This compound lacks a carbonyl group at the C-6 of the nitrogen ring of naphthalimide and in

TABLE I IC_{50} and K_D values for ADPRT inhibitors

Compound	IC_{50}[a]	Binding constant[b] K_{D1}	Binding constant[b] K_{D2}
NAP	87 ± 12 nM	54 ± 6 nM	1.2 ± 0.1 μM
CMP1	195 ± 30 nM	135 ± 28 nM	
CMP2	1.0 ± 0.3 μM	474 ± 60 nM	
CMP3	1.0 ± 0.4 μM	264 ± 28 nM	
CMP4	1.5 ± 0.2 μM	9 ± 2 nM,	2.7 ± 0.6 μM
CMP5	>5 μM	ND[c]	
CMP6	7.0 ± 2 μM	26 ± 5 nM	2.0 ± 0.5 μM
CMP7	12 ± 3 μM	ND	
CMP8	>20 μM	3.0 ± 0.5 nM	
CMP9	121 ± 15 μM	1.3 ± 0.1 μM	
CMP10	>100 μM	20 ± 2.0 μM	
CMP11	139 ± 15 μM	269 ± 50 μM	
CMP12	484 ± 35 μM	34 ± 5 nM	50 ± 15 μM

[a] The IC_{50} values were determined as described in *Materials and Methods* from the fit of the dose-response curve for each inhibitor. [b] The binding constants, K_{D1} and K_{D2} were determined as described in *Materials and Methods* and the binding curves were fit to an equation for either a one-site or a two-site binding model. [c] ND, not determined. The results represent the mean ± the standard deviation and were calculated from two independent experiments with samples measured in triplicate.

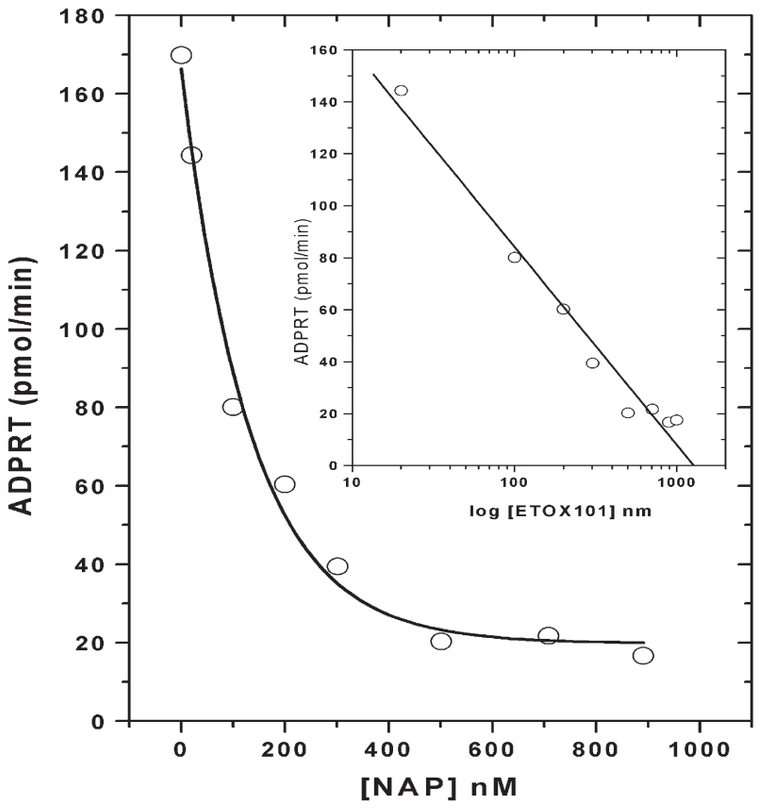

FIGURE 5 *Dose-response curve for NAP on the ADPRT activity of PE24.* Various aliquots of a stock solution of NAP prepared in DMSO and diluted using ethanol as a co-solvent with buffer (0.2% final, v/v) were pre-incubated with 1.25 μM PE24 for 10 min on ice. Subsequently, 10 μL of this solution was added to the ADPRT assay medium containing 20 mM TRIS–HCl, 50 mM NaCl, pH 7.9, 500 μM ϵ-NAD^+, and 20 μM eEF-2 at 25°C. The linear component of the kinetic traces was best fit by least squares regression analysis and plotted as shown above. The transformed data were then analyzed by nonlinear regression analysis (see *Materials and Methods* for details).

essence is deoxy NAP. Some inhibitors possess a K_{D2} value that can be correlated with their IC_{50} values (CMP4, CMP6, and CMP12). NAP possesses a K_{D2} value that is much higher than either its K_{D1} or IC_{50} value indicating that there may exist a NAP-binding site at a location removed from the active site that does not function as a modulation site for catalysis.

Dose-response Curve for NAP

The dose-response curve for NAP on the ADPRT activity of PE24 is shown in Figure 5. The IC_{50} value is near 100 nM (Table I) but a small amount of residual ADPRT activity (10% of the original) remains at 1000 nM NAP indicating that NAP is not capable of completely blocking the activity of PE24. At present, the reason for this observation is unclear (see *Discussion*) but may be related to the relative insolubility of NAP in aqueous solution. A semi-log plot of these data (Figure 5 inset) is linear with a correlation coefficient near 0.97, indicating that there is a single mechanism involved in the inhibition.

Inhibition Kinetics and Mechanism of NAP

Figure 6a shows the kinetics for the inhibition of ETA by NAP as plotted according to the Lineweaver-Burk method. The inhibition is clearly competitive since the V_{max} does not change but the K_M is affected by the presence of the inhibitor (increases) and the kinetic parameters, K_M and V_{max} are shown in Table II. The K_M values increase from 403 ± 40 μM (no NAP inhibitor) to 1584 ± 33 μM (200 nM NAP). A secondary plot for the inhibition data is shown in Figure 6b and the K_i as determined from these data was 90 ± 4 nM, in good agreement with the K_{D1} value (Table I). The competitive nature of the inhibitory effect by NAP on the ADPRT activity of PE24 indicates that this inhibitor binds within the nicotinamide-binding pocket as suggested by the modeling results (Figure 4), its structural similarity with nicotinamide, and previous results for PARP1-CF complexed with 4-amino-NAP.[22]

Reversible Nature of NAP Inhibition

The question of the reversible nature of the inhibition of PE24 ADPRT activity by NAP was addressed by

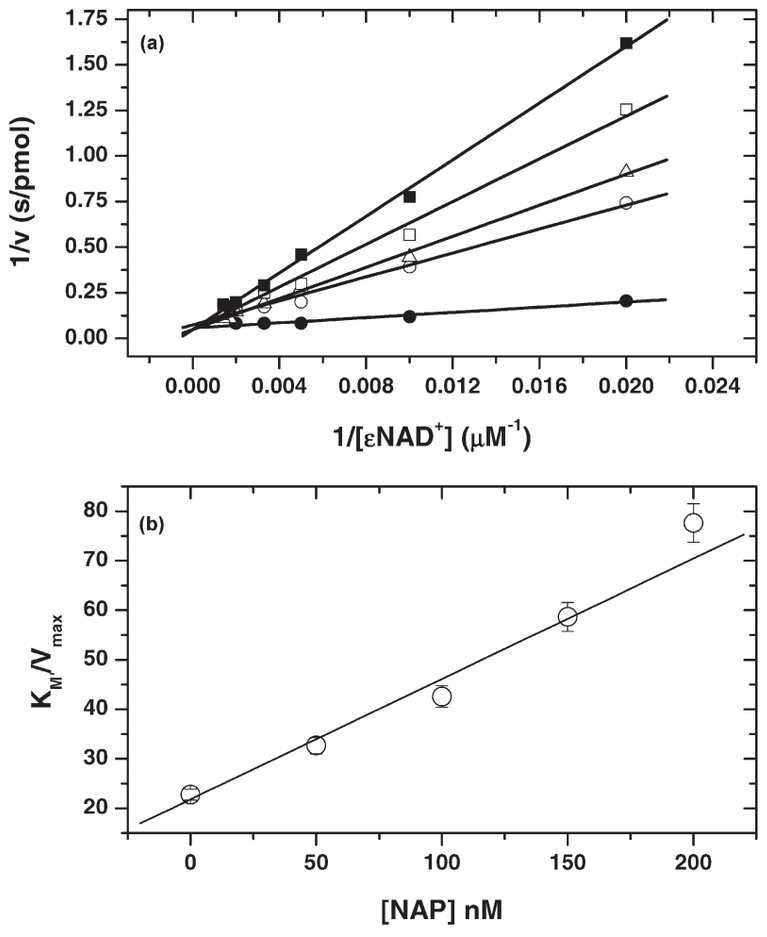

FIGURE 6 *Competitive inhibition of ADPRT activity by NAP. (a) Lineweaver-Burk plot of the inhibition of PE24 ADPRT activity at 0 (●), 50 (○), 100 (Δ), 150 (□), and 200 (■) nM NAP inhibitor. (b) Plot of the slope from (a) (K_M/V_{max}) against NAP concentration*. The assay included 20 mM TRIS–HCl, pH 7.9, 0–200 μM ϵ-NAD^+, 20 μM eEF-2, and 40 nM PE24 in a total volume of 70 μL. The reactions were initiated by the addition of enzyme and NAP that had been incubated prior to addition for 10 min. The progress curves were monitored for 5 min at 25°C (see *Materials and Methods* for details). The data are an average of 5 independent experiments each measured in triplicate.

incubation of the enzyme with a saturating level of NAP followed by exhaustive dialysis. The results of this test are shown in Table III. Dialysis alone (no inhibitor present) caused a loss of enzyme activity (nearly 50% decrease over 4 days with multiple buffer changes). However, the activity of the enzyme upon incubation with NAP was reduced to 20% of its original activity prior to dialysis. Upon dialysis, this activity was restored to 42% (Table III). Accounting for the intrinsic loss of enzyme activity during dialysis, the enzyme activity is restored to 90% of its full activity upon removal of the NAP inhibitor. These results suggest that the inhibition of ADPRT activity by NAP is reversible and is non-covalent in nature.

TABLE II K_M and V_{max} values for PE24 ADPRT in the presence of 1,8-naphthalimide

[NAP] (nM)	K_M (μM)	V_{max} (pmol/s)
0	403 ± 40	17.7 ± 2.2
50	442 ± 19	13.5 ± 2.1
100	881 ± 22	20.7 ± 3.9
150	1244 ± 55	21.2 ± 4.1
200	1584 ± 33	20.4 ± 4.6

The kinetic parameters K_M and V_{max} were determined from the inhibition data shown in Figure 6A. The kinetic data were acquired as described in *Materials and Methods* as previously documented (Armstrong and Merrill, 2001). The data shown are representative and represent the mean ± the standard deviation from three samples. The experiment was repeated four times with similar results.

TABLE III Dialysis test for reversible inhibition by 1,8 Naphthalimide of PE24 ADPRT activity

Sample	Dialysis	Inhibitor	ADPRT (pmol/min)
PE24	−	−	588 ± 90
PE24	+	−	299 ± 36
PE24	−	+	112 ± 10
PE24	+	+	246 ± 20

The dialysis experiment was conducted as described in detail in *Materials and Methods*. The results represent the mean ± the standard deviation from two separate experiments with samples measured in triplicate.

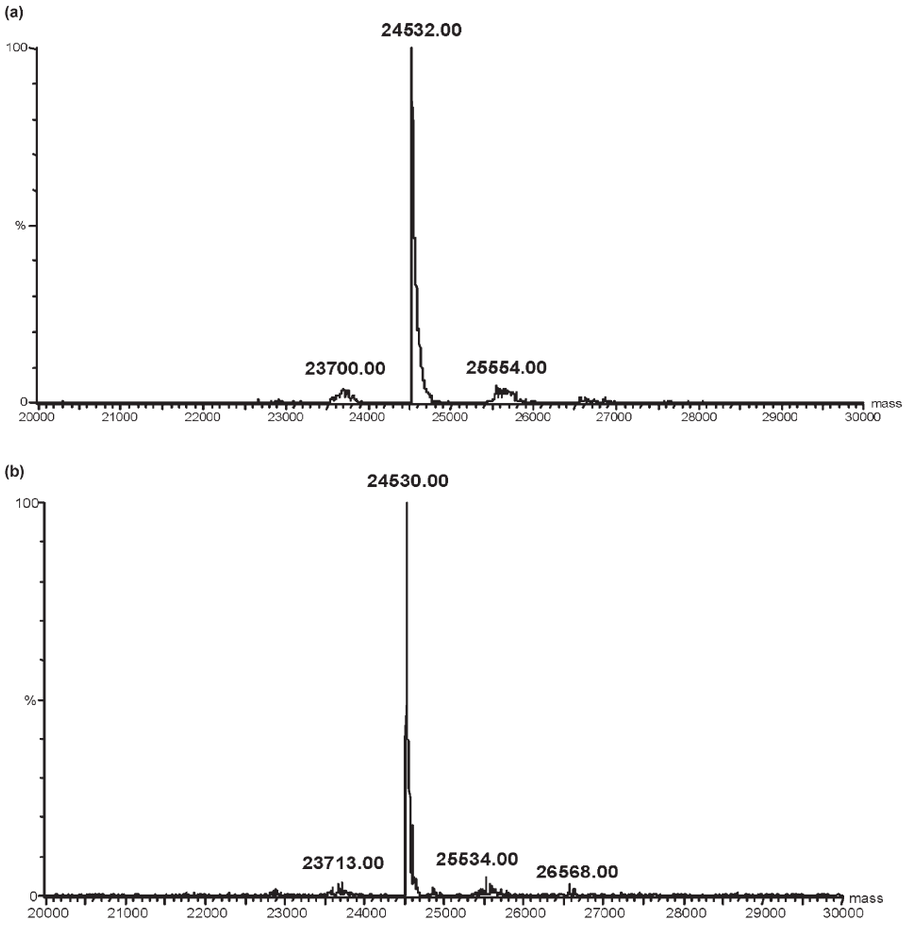

FIGURE 7 *Electrospray mass spectrometry spectra of PE24. (a) PE24 with no NAP inhibitor and (b) PE24 (40.8 μM) with 4.4 mM NAP for a molar ratio of NAP:PE24 of 100:1.* After incubation, the sample was lyophilized prior to ES-MS (see *Materials and Methods* for details). The abscissa corresponds to the mass of the sample in daltons.

Figure 7 shows the mass spectrometry results for a sample of PE24 (no NAP inhibitor present, Figure 7a) after incubation in the presence of a saturating concentration of NAP inhibitor (Figure 7b). The mass of PE24 (containing a 6-His tag at the C-terminus) alone is 24,532 ± 3 Da, in agreement with an earlier report by our laboratory,[28] and upon treatment with NAP there is no change in the mass of the protein peak (24,530 ± 3 Da, Figure 7b) with only one other small satellite peak seen at 24,600 Da. The expected mass for the covalent modification of PE24 by NAP is 24,727 Da for a single labeling or 24,924 for double labeling. It is believed that the small satellite peak is a minor contaminant picked up during the inhibitor incubation experiment.

Further evidence against the formation of a covalent PE24—NAP complex was demonstrated by incubation of NAP with the N-acetyl-tryptophan-amide standard (NATA). The NAD^+-binding assay for the inhibitors is based on the observation that NAD^+ quenches the Trp fluorescence of PE24,[27,29] indicating that these compounds bind very close to one or more of the Trp residues. This observation correlates well with our previous finding that NAD^+ preferentially quenches Trps 558 and 466 within the active site of the toxin.[27,29] Upon incubation of NATA with NAP, ^{1}H-NMR results indicated that there is no chemical reaction between these two compounds (data not shown) in support of the dialysis and mass spectrometry results.

DISCUSSION

It is reasonable to suggest from the data presented in this work that NAP and related compounds (including nicotinamide, Figure 1) function as relatively strong inhibitors of the ADPRT family of enzymes as previously suggested for PARPs.[21] These compounds inhibit these enzymes by competing with NAD^+ for the nicotinamide-binding site and reversibly bind to the enzyme with good to high affinity (Table I; Figure 5a and b). Within the group of compounds tested (Figure 1), it seems that the parent

NAP inhibitor is the most effective against ETA (Table I). Consequently, NAP was further characterized concerning its mechanism of inhibition. The data shown in Figure 6a indicate that NAP is a strong competitive inhibitor for the NAD^+ substrate with no change in the V_{max}, but a change (increase) in the K_M (Table II). Moreover, NAP inhibition is completely reversible, in that no trace of a covalent complex was detected by ^{1}H-NMR and ES-MS. When accounting for the intrinsic loss of ADPRT activity encountered during exhaustive dialysis, the enzymatic activity of PE24 was also largely recovered (Table III).

CMP1 is also a potent inhibitor, and it differs from NAP in that it possesses a partially hydrolyzed imide ring with an acid functionality—essentially an additional hydroxyl at the C1 of naphthalene. CMP8 is very similar to NAP, except the former compound lacks a carbonyl at the C-8 position of the naphthalene ring, yet the former compound is a considerably less potent inhibitor. This indicates that possessing an H-bond acceptor at both positions may be an important feature of the transition state for the ADPRT reaction. However, CMP3 also lacks the carbonyl functionality of NAP yet this compound shows remarkable potency (1.0 μM, IC_{50}) compared with CMP8 (~20 μM, IC_{50}), as is also the case for CMP2 ($IC_{50} = 1.0\,\mu M$). Bridging the phenyls of CMP3 with a methylene group (CMP9) causes a significant loss in inhibitor potency (~120 fold decrease). Amine substitution at the C-4 position of the naphthalene structure of NAP (CMP4) causes nearly a 20-fold loss in inhibition potential (Table I). Furthermore, if the inhibitor ring structure becomes too large and bulky the potency declines, indicating that the nicotinamide-binding pocket is likely the residence for most of the compounds shown in Figure 1, and that it is quite selective for nonpolar aromatic ring compounds with the potential to H-bond at one end of the structure. In summary, the most effective inhibitors possess aromaticity and a planar structure with some potential for H-bonding in the form of carbonyl and amine groups. However, effective inhibition is not a matter of simply displacing/competing with nicotinamide for the binding pocket since CMP8 is not nearly as potent (Group 2, see *Results* section) as the Group 1 inhibitors and it is less potent than CMP3, both of which lack a second carbonyl for H-bond interactions. These results suggest that the Group 1 inhibitors are functioning as competitive inhibitors for naphalimide and possess chemical structures that are mimicking the pre-transition-state species of the reaction (species that give rise to the transition-state for the reaction, although this latter species has not yet been identified). This idea is further supported by the relatively high affinity that NAP and CMP1 bind to the enzyme, i.e., these compounds bind with 1000-fold greater affinity than the NAD^+ substrate [Table I; [10]], which is the hallmark for a good inhibitor. The nature of the transition-state species for the ADPRT reaction catalyzed by mono-ADPRTs is currently poorly understood since it involves at least a portion of the protein substrate, eEF-2, including its diphthamide residue.[30] An additional piece of evidence concerning the nature of the binding of this group of inhibitors to PE24 was shown in Figure 3, where it was found that all the inhibitors quench the intrinsic fluorescence of the PE24 protein. The nature of the quenching was similar to that observed upon NAD^+ binding to the enzyme[27,29] (Table I).

The model of NAP bound to the enzyme was generated in order to provide clues as to the nature of the association between toxin and this high affinity inhibitor. Docking the inhibitor within the active site was naturally guided by the structural similarities that NAP shares with the nicotinamide moiety of the NAD^+ substrate for the toxin. The toxin-inhibitor structure was readily energy minimized in a conformation that mimicked the known structure of an NAD^+ analogue bound to this enzyme[12] as well as the structure of intact NAD^+ bound to DT,[25] which added greater credence to the proposal that these inhibitors mimic the nicotinamide portion of the NAD^+ substrate. Additionally, the X-ray structure of CMP4, 4-amino NAP (Figure 1), along with a related group of compounds, was determined for the catalytic domain of chicken PARP1, PARP1-CF. In the PARP1-inhibitor structure, 4-amino NAP binds to the well-defined nicotinamide subsite of the NAD^+-binding pocket. Notably, H-bonding was observed between Gly 863 and Ser 904 (corresponding to Gly 441 and Ala 478 in PE24) and the inhibitor amide group on 4-amino NAP. The model shown in Figure 4 indicates that Gly 441 likely does H-bond with the amide carbonyl of NAP but the Ser 904 in PARP1 is not conserved among these enzymes, it is replaced with Ala residues in both ETA and DT, perhaps indicating areas of potential discrimination in the design of inhibitors among the various ADPRT family members.

Unfortunately, no structural data exists for the ternary complex consisting of toxin, NAD^+, and eEF-2. Furthermore, there is little structural data for eEF-2 and in particular, the structure of the protein in the vicinity of the diphthamide residue is a speculative subject, at best. Presently, the best structure currently available is a 17.5 Å image determined by electron microscopy.[31] Consequently, there is not much evidence concerning the structure of the transition-state for the reaction, which leaves as the best current approach, one that probes the active site structure using a series of rationally designed inhibitor compounds while awaiting both structural and kinetic characterization

of the transition-state species for the reaction catalyzed by the ADPRT family.

Acknowledgements

We thank Dr Gary Dmitrienko for kindly providing access to Silicon Graphics™ computer modeling services at the University of Waterloo. We express appreciation to Gerry Prentice for expert technical assistance during the course of this work. We also thank Gilles Lajoie for performing the ES-MS analysis of various samples. We are also indebted to Dr Adrian Schwan for critical reading of the manuscript.

References

[1] Diekema, D.J., Pfaller, M.A., Jones, R.N., Doern, G.V., Winokur, P.L., Gales, A.C., Sader, H.S., Kugler, K. and Beach, M. (1999) *Clin. Infect. Dis.* **29**, 595–607.
[2] Richards, M.J., Edwards, J.R., Culver, D.H. and Gaynes, R.P. (1999) *Crit. Care Med.* **27**, 887–892.
[3] Tang, H.B., DiMango, D., Bryan, R., Gambello, M., Iglewski, B.H., Goldberg, J.B. and Prince, A. (1996) *Infect. Immun.* **64**, 37–43.
[4] FitzGerald, D., Morris, R.E. and Saelinger, C.B. (1980) *Cell* **21**, 867–873.
[5] Kounnas, M.Z., Morris, R.E., Thompson, M.R., FitzGerald, D.J., Strickland, D.K. and Saelinger, C.B. (1992) *J. Biol. Chem.* **267**, 12420–12423.
[6] Seetharam, S., Chaudhary, V.K., FitzGerald, D. and Pastan, I. (1991) *J. Biol. Chem.* **266**, 17376–17381.
[7] Alami, M., Taupiac, M.-P., Reggio, H., Bienvenue, A. and Beaumelle, B. (1998) *Mol. Cell. Biol.* **9**, 387–402.
[8] Foley, B.T., Hoehring, J.M. and Moehring, T.J. (1995) *J. Biol. Chem.* **270**, 23218–23225.
[9] Nygard, O. and Nilsson, L. (1990) *Eur. J. Biochem.* **191**, 1–17.
[10] Armstrong, S.A. and Merrill, A.R. (2001) *Anal. Biochem.* **292**, 26–33.
[11] Li, M., Dyda, F., Benhar, I., Pastan, I. and Davies, D.R. (1995) *Proc. Natl Acad. Sci. USA* **92**, 9308–9312.
[12] Li, M., Dyda, F., Benhar, I., Pastan, I. and Davies, D.R. (1996) *Proc. Natl Acad. Sci. USA* **93**, 6902–6906.
[13] Koch-Nolte, F. and Haag, F. (1997) In: Koch-Nolte, F. and Haag, F., eds, *ADP-ribosylation in Animal Tissue* (Plenum Press, NY), pp. 1–13.
[14] Prentice, G.A., Roberts, T.M. and Merrill, A.R. (2001) *Protein Sci.* **10**(Suppl.), 409a.
[15] Bell, C.E., Yeates, T.O. and Eisenberg, D. (1997) *Protein Sci.* **6**, 2084–2096.
[16] Zhang, J. (1999) *Emerging Drugs* **4**, 209–221.
[17] Jacobson, M.K. and Jacobson, E.L. (1999) *Trends Biochem. Sci.* **24**, 415–417.
[18] Gasteiger, J. and Marsili, M. (1980) *Tetrahedron* **36**, 3219–3228.
[19] Li, Jia-He and Zhang, J. (2001) *Idrugs* **4**, 804–812.
[20] Banasik, M. and Ueda, K. (1994) *Mol. Cell Biochem.* **138**, 185–197.
[21] Schlicker, A., Peschke, P., Burkle, A., Hahn, E.W. and Kim, J.H. (1999) *Intl. J. Rad. Biol.* **75**, 91–100.
[22] Ruf, A., de Murcia, G. and Schultz, G.E. (1998) *Biochemistry* **37**, 3893–3900.
[23] Wozniak, D.J., Hsu, L.Y. and Galloway (1988) *Proc. Natl Acad. Sci. USA* **85**, 8880–8884.
[24] McGowan, J.L., Kessler, S.P., Anderson, D.C. and Galloway, D.R. (1990) *J. Biol. Chem.* **266**, 4911–4916.
[25] Bell, C.E. and Eisenberg, D. (1996) *Biochemistry* **35**, 1137–1149.
[26] Yates, S. Merrill, A.R. (2001) *J. Biol. Chem.* **276**, 35029–35036.
[27] Beattie, B.K., Prentice, G.A. and Merrill, A.R. (1996) *Biochemistry* **35**, 15134–15142.
[28] Mohammadi, F. and Merrill, A.R. (2001) *Biochemistry* **40**, 10273–10283.
[29] Beattie, B.K. and Merrill, A.R. (1999) *J. Biol. Chem.* **274**, 15646–15654.
[30] Berti, P.J., Blanke, S.R. and Schramm, V.L. (1997) *J. Am. Chem. Soc.* **119**, 12079–12088.
[31] Gomez-Lorenzo, M.G., Spahn, C.M., Agrawal, R.K., Grassucci, R.A., Penczek, P., Chakraburtty, K., Ballesta, J.P., Lavandera, J.L., Garcia-Bustos, J.F. and Frank, J. (2000) *EMBO J.* **19**, 2710–2718.